Thermal imaging of rapidly evaporating saltwater drops

Samuel Valley[1] & Cody J. Brownell[1,*]
1: Mechanical Engineering Dept., The United States Naval Academy, USA
* Corresponding author: brownell@usna.edu

Keywords: Drop Evaporation, Laser Heating, Acoustic Levitation, Thermal Imaging

ABSTRACT

Use of high energy lasers in the maritime environment may involve interactions betweeen a laser beam and liquid water in the form of rain or sea spray. During these interactions, the drop thermodynamics and the optical propagation of the laser are coupled through the absorption-dependent vaporization process. Experiments on single, acoustically levitated, saltwater drops (initial diameter $D_o \geq 1$mm) are conducted where a high energy NIR laser is used to irradiate and heat a drop into a rapid evaporation regime. An IR camera is used to measure drop volume and surface temperature during and after the heating process. Measured vaporization rate is compared to a model for vaporization of fresh water drops in the same regime. Determinants of mean surface temperature are discussed, and are compared to previous experiments with large fresh water drops and model predictions for laser heating of small aqueous aerosols.

---

1. Introduction

Naval applications of high energy lasers, for either weapons or communication, pose significant challenges due to the complexity of the maritime environment. Liquid water drops from fog, rain, or sea spray may interfere with beam transmission (O'Rourke 2014). On the defensive side, the observed challenges to laser weapons imposed by liquid water present an opportunity, as it may be possible for a small watercraft or a drone to hide in fog, rain, or sea spray.

Previous experimental research on droplet heating with lasers has usually used CO_2 lasers with a 10-micron wavelength, and has focused on very small fresh water samples. The absorptivity of liquid water at this wavelength is high, so heating effects can be drastic. Heating of small aqueous aerosols with CO_2 lasers found two distinct heating regimes, a "slow" regime where the heat led to rapid evaporation of the droplet and a "fast" regime where a single laser pulse resulted in explosive vaporization (Armstrong 1984, 1986, & 1989; Carls 1987; Sprangle 2005; Zardecki 1998). Other work investigated the effects of irradiated droplets for the application of cloud clearance, using droplets with diameters from 1-140 μm (Kafalas 1973). For drops greater than 100 μm in diameter, single drop experiments with liquid fuels have been conducted with combustion-related

applications (Saha 2012a&b). Previous work by the authors has looked at vaporization rates for fresh water drops, which validated the use of vaporization rate models for small aqueous aerosols for larger drops under certain conditions (Brownell 2017; Tracey 2018).

2. Theory

Comparing the heating of a large drop (initial diameter $D_o \geq$ 1-mm) to small aqueous aerosols, three key assumptions for aerosol heating need to be re-assessed: i) use of Mie absorption coefficient, ii) isothermal drop, and iii) uniform heating. However, when considering an energy balance integrated over the entire liquid drop, only the rate of absorbed energy needs to be included. For the case where thermal conduction can be neglected, a quasi-equilibrium process will be observed where the absorbed laser power equals the rate of energy leaving the drop due to evaporation (Davies 1987). According to Williams (1965):

$$-h_{fg}\, dM/dt = 4/3\, \pi R^3 \alpha I_o \qquad (1)$$

where the left side is the product of the enthalpy of vaporization and the evaporation rate, and the right side is the rate of absorbed laser energy. Writing $dM/dt = \rho_D 4\pi R^2\, dR/dt$, this can be recast and solved for radius as a funtion of time $R(t)$:

$$R = R_o exp\left[-\left(\alpha I_o / 3\rho_D h_{fg}\right)t\right] \qquad (2)$$

If the equilibrium vaporization rate is set strictly through the equation above, it is largely independent of the drop temperature. Drop surface temperature is then set through the Hertz-Knudsen equation to the level required to drive the above evaporation rate. With a large drop, however, the interface is far from isothermal and the surface temperature is affected by advection of hot eddies from the interior of the drop to the surface. Because diffusive mechanisms, while important, do not dominate the interior drop dynamics, spatial and temporal fluctuations in surface temperature are present. The subsequent effects of a dynamic drop interface on the evaporation of the water is not well understood.

The focus of this work is laser interaction with "large" salt water drops, with initial diameter greater than 1-mm, such as sea spray. Absorption in water depends strongly upon impurities within the water, and it is difficult to predict absorption a priori for a naturally obtained sample. The salt content in pure sea water is nominally 35 parts per thousand by weight (Mobley 1994).

Solubility of salt in water varies only slightly with temperature, and is 370 parts per thousand at 60°C (IUPAC-NIST). Salts in sea water have a negligible effect on absorption except at very long wavelengths; the effect of salts on scattering is more significant.

3. Experiment

A series of experiments involving acoustically levitated, irradiated drops is presented. Figure 1 shows a schematic of the overall experimental setup, located at the Naval Academy's Directed Energy Research Center (DERC). The drops in this experiment were suspended by a tec5 AG ultrasonic levitator. The size of the drops levitated depends on the wavelength of the sonic wave used to create the pressure nodes. The optimal drop diameter is given as $d_s = \lambda/3$, where λ is the acoustic wavelength, as this is the diameter that requires the minimum power to levitate the drop. The standard operating parameters for the levitator are an acoustic wavelength of about 5.9 mm and a frequency of 58 kHz, making the optimal drop size approximately 2 mm (tec5 2014). The acoustic energy density profile surrounding the levitated drop causes the drop to deform and take on an oblate spheroid appearance. This is a result of the balancing of capillary and gravitation forces experienced by the drop during its levitation. In practice, the ellipticity $e = [1 - c^2/a^2]$ of drops varied from 0.7 to 0.99, with higher ellipticities (rounder drops) at smaller sizes. Figure 2 shows an image of a typical drop in the acoustic levitator.

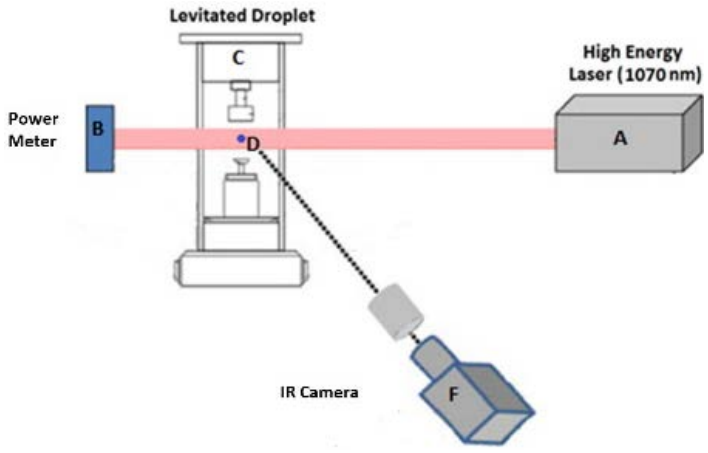

Fig. 1 Experiment Schematic.

The laser used in this experiment is a 100-W IPG High Power Fiber laser. The output beam power and profile was measured before the experiments to confirm specifications. The laser output at full power was 107 W, and the maximum $1/e^2$ beam diameter at the target was 5.28 mm. Because the drops used in these experiments are smaller than the beam diameter, the average irradiance

incident upon the drop is larger than the mean irradiance value, and will change by ~5% as the drop vaporizes and shrinks. The peak intensity for a Gaussian beam with these characteristics is 977 W/cm^2, and 900 W/cm^2 is a representative value for irradiance incident on the drop at full power.

Integrated beam power is collected at the terminus of the laser with a thermopile. The drop surface is imaged with a FLIR SC6100, factory calibrated to a temperature range of 10^{o}C – 90^{o}C. Emissivity of water was determined through separate experiments using ice and boiling water baths at a range of incidence angles. In addition to the equipment shown in the schematic, a Jasco V-670 Model ISN-723 integrating sphere was used to determine absorptivity for the water samples tested.

Each "run" consists of a 60-sec laser exposure, and 75-sec of IR video at a frame rate of 30 Hz encompassing the brief transient heat-up, quasi-equilibrium evaporation, and, if possible, the cool down period. (A number of drops get “lost” before the laser strike is finished.) The results presented below are drawn from a data set consisting of eight (8) runs with fresh water drops, and ninteen (19) runs with salt water drops. The salt water samples are made in bulk by dissolving salt at 35 ppt in heated fresh water, and letting it cool for at least two hours before testing. For both fresh and salt water, a micropipette is used to place a single drop from a bulk reservoir into the levitator. The initial size of the drop in the levitator, determined from image calibrations, ranged from 0.95-mm^3 to 8.5-mm^3 with a mean of 4.75-mm^3. (In diameter, this corresponds to a range of 1.2-mm to 2.5-mm.) Image resolution varied slightly from run to run, but was typically around 0.02 mm/pix. Ambient temperature, barometric pressure, and relative humidity were also recorded.

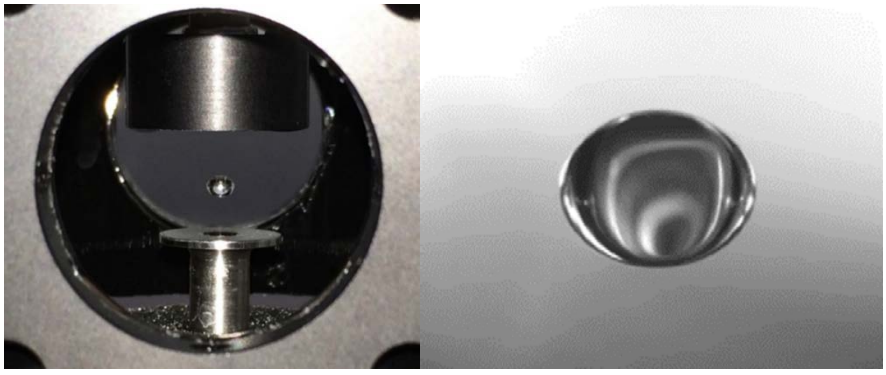

Fig. 2 A drop in the levitator. Drop diameter is approximately 1.5-mm in both images.

4. Results

Sample IR camera images are shown in Fig. 3. The drops in the images are 2.0-mm diameter, shown about 4-sec after lasing begins. A thin region around the perimeter of the drop is noticeable where the temperature data is unreliable due to the incidence angle. Away from the perimeter, however, calibrations confirmed little change in emissivity with angle.

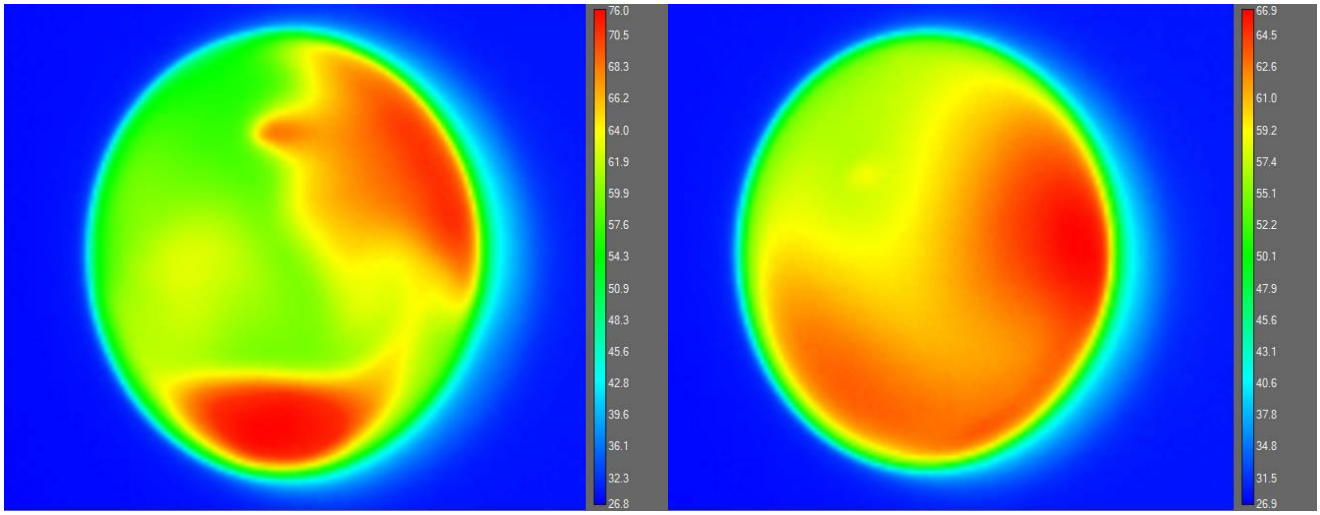

Fig. 3 Sample images showing drop surface temperature.

Figure 4 shows drop volume vs time for a characteristic fresh water run and a characteristic salt water run. These particular runs were chosen for comparison because of the similar initial drop size. Drop volume is calculated assuming symmetry about the vertical axis: $V = 4/3\pi a^2 c$ where a is drop radius in the horizontal and c is drop radius in the vertical direction. Note that the initial volume has greater uncertainty because the drop blends into the surroundings when at ambient temperature. Taken from the same runs, Fig. 5 shows relative surface temperature vs time. The relative surface temperature is the mean value from a 3x3 pixel region at the center of the drop image, with the ambient temperature subtracted out. In the fresh water case, the drop temperature quickly reaches its quasi-equilibrium value, where the temperature is set from the Hertz-Knudsen equation based on what is required to drive the evaporation. In the fresh water case, a qualitative observation is a reduction in temperature variance as the drop shrinks. While the salt water drop initially behaves like the fresh drop, irradiated salt water drops will reach a threshold where the measured temperature spikes dramatically. This is often coupled with some instability of the drop within the levitator. The hypothesis for this phenomenon is that enough water has evaporated such that the drop reaches its solubility limit, and salt begins to come out of solution. Solid salt particles have dramatically higher absorptivities, resulting in much higher observed temperatures.

This also explains the flattening of the volume vs time curve for salt water in Fig. 4. When the salt precipitates the solid salt crystal dramatically increases laser absorption, and the remaining liquid soon evaporates. A solid ball of low-density salt then remains, which does not experience further changes in volume. At this point the temperature data is unreliable, due to the change in emissivity accompanying the change in the visible surface.

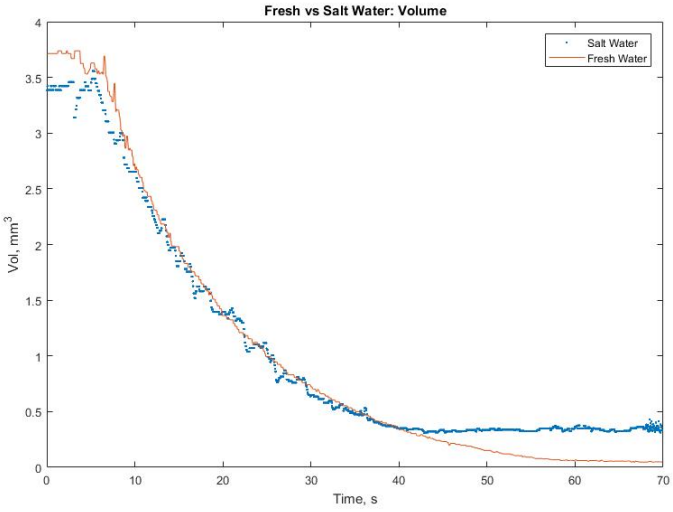

Fig. 4 Comparison of Volume vs Time for representative laser strikes on fresh (--)and salt (·) water.

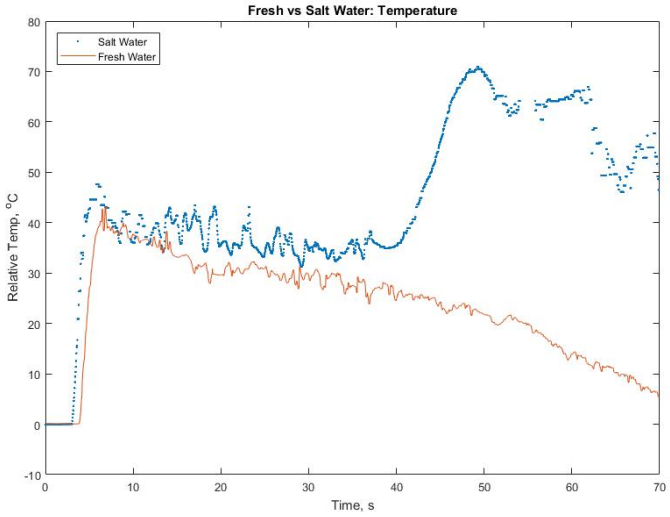

Fig. 5 Comparison of relative temperature vs time for representative laser strikes on fresh (--)and salt (·) water.

5. Analysis and Discussion

The volume threshold for the drop temperature spike is likely caused by the drop reaching its solubility limit as water leaves the system. For an initial water sample that is mixed to 13% of the

solubility limit, this transition would occur when the drop diameter is 51% of the initial diameter; using our previous vaporization rate model, this would occur around t = 42s under given conditions, approximately what is seen in Fig. 5 above. In Fig. 6, a subset of the salt water runs are selected where the transition to a different regime is rapid and can clearly be identified. For these samples, the drop volume at the time of the transition is plotted vs the initial drop volume. Alongside the data, the volume ratio of 0.135 is shown which corresponds to the expected volume ratio at the time salt saturation is reached assuming an initial salinity of 3.5% and saturation at 26%. The figure shows good agreement to this expected volume ratio; the variance is likely due to uncertainty in the initial mixture or changes in the saturation limit with drop temperature. With very small salt water aerosols, drops will have less internal mixing, salinity may be higher at the outside vs the middle of the drop, and the local solubility limit may be reached at the surface even if the total salt content of the drop is lower. This has not been observed in the present data, where all drops are significantly larger than suspended aerosols in the atmosphere.

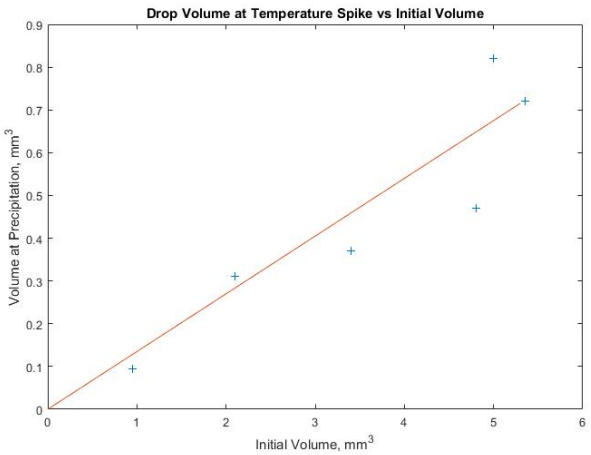

Fig. 6 Initial drop volume vs volume at temperature spike. The straight line indicates a volume ratio of 0.135, corresponding to the ratio of the initial salt concentration (3.5%) to the saturation limit at typical drop temperatures (26%). Only a subset of data where the temperature spike could clearly be identified is plotted.

Because of the complex nature of the available data - where each drop has a different initial volume, the volume changes through a quasi-equilibrium process with finite duration, and drops occasionally see intermittent instability within the apparatus - analysis of drop temperature is performed in a way that reduces the effect of outliers in the data. First, drop temperature at the center of each image is pulled as before (Fig. 5) from a 3x3 pixel region for each video frame. The ambient (initial) temperature is subtracted out, leaving the temperature of the drop surface relative to the surroundings. (The initial temperatures varied between 16.7°C and 22.4°C.) Because of interest in the variance of the drop temperature and because the temperature is not stationary, a

low-pass filter with a cutoff frequency of 1-Hz is applied to the temperature vs time data for each run. A high frequency 'variance' is then calculated for each frame as the square of the difference between the actual and filtered relative temperatures. For each run, plots of relative temperature vs time and drop volume vs time are then manually examined to identify the frame range(s) where the drop is in a quasi-equilibrium evaporation regime and where there are no obvious instabilities of the drop within the levitator. For data regions that meet these requirements, the drop relative temperature and the temperature variance are placed in bins according to the drop volume at that time. Several bin sizes were checked for consistency, with little effect on the overall trends. In the figures below, the volume bins range from [0.0 mm^3 - 0.5 mm^3] at the low end up to [> 4.5mm^3] at the high end. Using this distribution, each bin has at least 614 entries, and the average number of entries per bin is 976.

Figure 7 shows the average (median) relative temperature in each volume bin. While the expected result was that smaller drops would have smaller relative temperatures, the data shows that this is only true for small drops (volume less than ~1.5 mm^3) and that for larger drops, the relative surface temperature is quite constant over a wide range of sizes. The expectation was based on the assumption of an energy balance between laser absorption, which scales with diameter as D^3, and evaporation, which scales as D^2. This balance would necessitate higher surface temperatures to drive the evaporation process at larger diameters. There are several possible reasons why the equilibrium temperature becomes constant large volume. This could be due to the Gaussian profile of the laser beam, and the fact that the additional exposed volume for a larger drop is on the periphery of the beam. While all drops examined are well below the $1/e^2$ beam width, at large drop diameter perhaps the assumption of uniform irradiance is no longer valid. The temperature behavior could also be due to a greater departure from isothermal conditions. While none of these drops are spatially isothermal, there is likely a greater temperature difference between the drop center and drop surface for the larger drops. While interior drop temperatures were not measured here, CFD of the laser drop interaction is ongoing and will provide some answers.

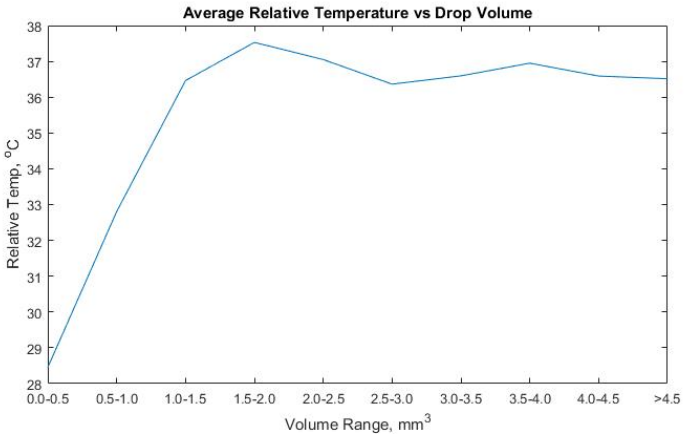

Fig. 7 Median drop surface temperature vs volume bin during the quasi-equilibrium heating phase.

Temperature fluctuations, characterized as the median value of the temperature variance within a volume bin, is plotted as a function of volume in Fig. 8. The quantity captured in the figure is not a true variance, as it is a median of the square of the difference from an expected value, but this analysis does a superior job of handling outliers. Because the expected value was calculated from filtered data, this quantity also only captures variance at frequencies below the filter frequency of 1 Hz. From the figure, no clear relationship between high-frequency temperature fluctuations and drop volume can be seen. The expectations were that smaller drops, where the effects of viscosity are greater, will see smaller fluctuations in temperature than larger drops. This analysis has not yet been conducted on the fresh water runs. It is possible that larger than expected fluctuations for the smaller drops are related to those drop sizes occurring at the end of the laser strike, when the salt content is close to saturation and is possibly beginning to come out of solution.

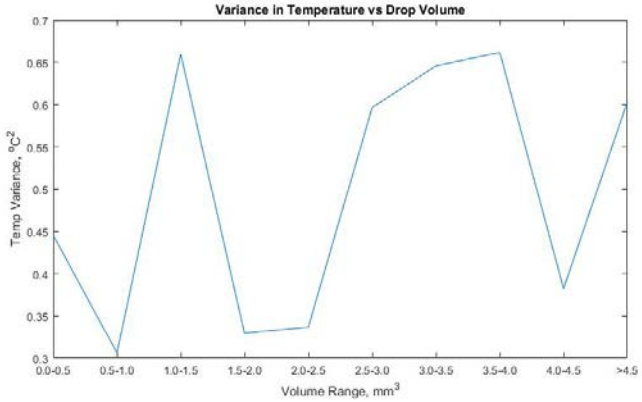

Fig. 8 Median variance from expected temperature vs volume bin during the quasi-equilibrium heating phase. No clear relationship is seen via this analysis.

Along with a comparson of the variance to fresh water data, the next step is to use the 2D nature of the imaging data collected to explicitly measure the size of the visible scalar structures. Large

temperature fluctuations that are due to a decreased role for viscosity and diffusive processes may correlate with smaller scalar structures and thinner scalar gradient regions. This quantity can be extracted from the imaging data and placed in volume bins in much the same way as the temperature and temperature variance were. Uniformity in the structure of the temperature field would provide an additional confirmation of the relationship between temperature fluctuations and drop volume.

6. Conclusions

For irradiated water drops, several comparisons for fresh vs salt water show similar initial evaporation processes, followed by a distinct divergence in drop temperatures at the point where the salt begins to precipitate. The equilibrium drop temperature during the evaporation phase is found to depend on drop size for small drops, but results for larger drops are unclear. Counter to initial expectations, the high-frequency variance in drop surface temperature does not have a clear relationship to drop size. Further analysis of the spatial data is needed to confirm this.

The conditions under which nucleate boiling will occur and the effects this has on relevant processes needs to be examined further. Peak temperatures are located in the drop interior, and are inaccessable using traditional imaging methods. Because calcuations of drop temperature may require a Navier-Stokes solution within the drop, predictions of either instantaneous or mean drop temperature are not trivial.

Acknowledgements

The authors are grateful for support from the ONR Code 35 (Ryan Hoffman and Peter Morrison), HEL-JTO (Harro Ackermann), and DEPS (Mark Niece).

References

Armstrong, R.L. (1984) Aerosol heating and vaporization by pulsed light beams. Appl Opt 23:148-155.

Armstrong, R.L., O'Rourke, P.J., and Zardecki, A. (1986) Vaporization of irradiated droplets. Phys Fluds 29:3573-3581.

Armstrong, R.L and Park, B.S. (1989) Laser Droplet Heating: Fast and Slow Regimes. Appl Opt 28:3671-3680.

Basics About Ultrasonic Levitation. (2014) In Ultrasonic Levitator Manual. Germany: Tec5-Technology for Spectroscopy.

Brownell, C.J., Tracey, T.E., and Payne, N. (2017) Imaging of large water drops during laser heating and vaporization. OSA Imaging and Applied Optics Congress, Propagation Through and Characterization of Atmospheric and Oceanic Phenomena, San Franciso, CA. doi: 10.1364/PCAOP.2017.PW3D.4

Carls, J.C., and Brock, J.R. (1987) Explosion of a water droplet by pulsed laser heating. Aerosol Sci Tech 7:79-90.

Davies, S.C., and Brock, J.R. (1987) Laser evaporation of droplets. Appl Opt 26:786-793.

IUPAC-NIST Solubility Database. NIST Standard Reference Database 106. Online: srdata.nist.gov/solubility/ Referenced Dec 2017.

Kafalas, P., and Herrmann, J. (1973) Dynamics and energetics of the explosive vaporization of fog droplets by a 10.6 micron laser pulse. Appl Opt 12:772-775.

Mobley, C., (1994) Optical Properties of Water. In M. Bass (Ed.), Handbook of Optics (2nd ed.). McGraw Hill, New York, NY..

O'Rourke, R. (2014) Navy Shipboard Lasers for Surface, Air, And Missile Defense: Background and Issues for Congress. Congressional Research Service R41526.

Saha, A., Basu, S., and Kumar, R. (2012) Particle image velocimetry and infrared thermography in a levitated droplet with nanosilica suspensions. Exp Fluids 52:795-807.

Saha, A., Basu, S., and Kumar, R. (2012) Scaling analysis: equivalence of convective and radiative heating of levitated droplet. Appl Phys Lett 100:204104.

Sprangle, P., Peñano, J., and Hafizi, B. (2005) Optimum wavelength and power for efficient laser propagation in various atmospheric environments. Report No. NRL/MR/6790-05-8907.

Tracey, T.E., and Brownell, C.J. (2018) Evaporation and beam profile measurements on an irradiated water drop. J of Directed Energy 1.

Williams, F.A. (1965) On vaporization of mist by radiation. Int J of Heat and Mass Trans 8:575-587.

Zardecki, A., and Armstrong, R.L. (1998) Energy balance in laser-irradiated vaporizing droplets. Appl Opt 27:3690-3695.